ACS APPLIED MATERIALS & INTERFACES

Research Article

www.acsami.org

Synthesis and Cellular Internalization of Spindle Hematite/Polymer Hybrid Nanoparticles

Jing Wang,[†] Wen Zhu,*[,†] Lixin Liu,*[,‡] Yongming Chen,*[,†,‡] and Chun Wang[§]

[†]Laboratory of Polymer Physics and Chemistry, Institute of Chemistry, The Chinese Academy of Sciences, Beijing 100190, China

[‡]Key Laboratory of the Ministry of Education for Polymer Composite and Functional Materials, Department of Polymer and Materials Science, School of Chemistry and Chemical Engineering, Sun Yat-Sen University, Guangzhou 510275, China

[§]Department of Biomedical Engineering, University of Minnesota, Minneapolis, Minnesota 55455, United States

ABSTRACT: Nonspherical spindle-shaped hematite/polymer hybrid nanoparticles (SPNPs) were synthesized via surface-initiated atom transfer radical polymerization (SI-ATRP). The long axis of the SPNPs was 370 ± 65 nm, and the short axis was 80 ± 15 nm with an aspect ratio of 4.6−4.7. The SPNPs were characterized by transmission electron microscopy (TEM), Fourier transform infrared spectroscopy (FT-IR), and X-ray photoelectron spectroscopy (XPS). Thermogravimetric analysis (TGA) was used to estimate the content of grafted polymer. Light-scattering measurement was used to detect the particle size distribution of SPNPs in water and in cell culture medium. HeLa cells internalized the SPNPs within 1 h, and the uptake reached equilibrium in 8 h. These observations contribute to better understanding of the interactions between nonspherical nanoparticles and cells, which may have implication for designing drug delivery vehicles.

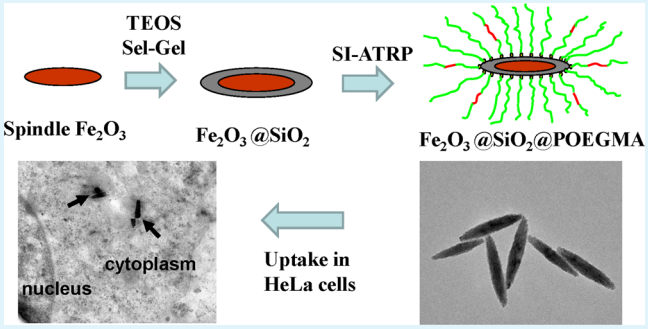

KEYWORDS: *cellular internalization, grafted polymers, HeLa cells, hematite nanoparticles, nonspherical particles*

1. INTRODUCTION

Polymeric nanoparticles have attracted considerable attention for drug delivery applications because of their unique properties in enhancing bioavailability of medicine.[1−5] A pioneering study by Savić et al. reported on spherical micelles self-assembled by fluorescently labeled poly(ethylene oxide)-*b*-poly(ε-caprolactone) (PEO-*b*-PCL) and investigated their intracellular distribution, providing a biological basis for polymeric nanoparticles as intracellular drug delivery vehicles.[6] Since then, much of the research has focused on the investigation of spherical nanoparticles. In recent years, nonspherical nanoparticles have shown certain advantages over spherical ones as more efficient drug carriers. Geng et al. reported that PEO-*b*-PCL and poly(ethylene oxide)-*b*-poly(ethyl ethylene) (PEO-*b*-PEE) filomicelles exhibited several times longer blood circulation in rats compared to spherical micelles of the same composition.[7] Gratton et al. reported that cylindrical nanoparticles synthesized by the particle replication in nonwetting templates (PRINT) method with a high aspect ratio of 3 (height × diameter: 450 nm × 150 nm) were internalized by HeLa cells at a rate 4 times faster than particles with a low aspect ratio of 1 (height × diameter: 200 nm × 200 nm).[8] Meng et al. demonstrated that mesoporous silica nanoparticles (MSNP) with an aspect ratio of 2.1−2.5 were taken up in larger quantities by HeLa cells compared to shorter or longer silica nanorods.[9] Hao et al. reported that the long MSNP could be used as ideal antioxidant carriers to protect cells from oxidative injury because the A375 cells treated by long MSNP had relatively low intracellular reactive oxygen species concentration in the presence and absence of serum proteins.[10] Chen et al. fabricated multifunctional mesoporous nanoellipsoids to use as drug carriers and contrast agents for magnetic resonance imaging (MRI). It is found that these nonspherical nanoparticles can load doxorubicin and can demonstrate the relatively high r_2 value.[11] Zhang et al. found that the polystyrene nanodisks showed less perturbation to cells than nanospheres.[12] Fan et al. found that the nanoparticles based on poly(lactide-*co*-glycolide-*b*-ethylene glycol-*b*-lactide-*co*-glycolide) triblock copolymers of a different shape showed greater enhanced properties including drug release, endocytosis, and intracellular accumulation compared to spherical ones.[13] Nonspherical particles have several unique features and properties, including longer blood circulation times,[7] faster internalization rate,[8,9,14,15] different uptake mechanism,[16,17] specific organ distribution,[18−21] and complex motions under flow conditions.[22−24] When interacting with proteins and cells, spherical and nonspherical nanoparticles have different surface area for contact and different kinetics and energetics of binding. These findings suggest that the shape of the particles is a key design parameter for drug carriers. Furthermore, some theoretical studies have confirmed the unique properties of the nonspherical particles. Nangia et al. used the molecular

Received: December 29, 2014
Accepted: February 17, 2015
Published: February 17, 2015

DOI: 10.1021/am509152h
ACS Appl. Mater. Interfaces 2015, 7, 5454−5461

Scheme 1. Synthesis of Nonspherical SPNPs with α-Fe_2O_3 Core and Fluorescent Shell of POEGMA Brushes by Surface-Initiated ATRP

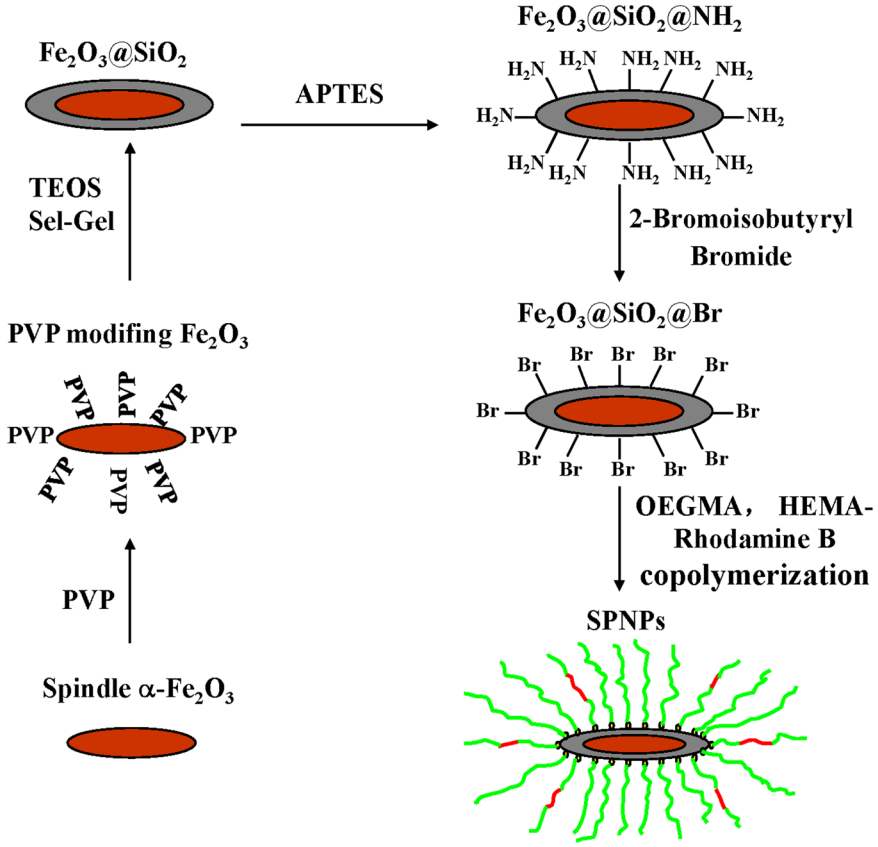

dynamics simulation techniques to find that the translocation rates of cone-, cube-, rod-, rice-, pyramid-, and sphere-shaped nanoparticles through lipid membranes can span a larger scale, and the rates were determined by the shape and the surface property of the particle.[25] Huang et al. applied a coarse-grained molecular dynamics model to find that the size of nanoparticles determined the process of endocytosis and whether it can be completed, while the shape of nanoparticles determined the endocytic pathway and the angle of uptake.[26]

Spindle hematite nanoparticles are biological nontoxic and can be prepared using simple methods. Monodisperse spindle α-Fe_2O_3 nanoparticles were first prepared via hydrolysis of iron(III) nitrate ($Fe(NO_3)_3$) with the addition of nitric acid (HNO_3) in aqueous solution by Matijević and Scheiner.[27] The aspect ratio of spindle α-Fe_2O_3 can be simply adjusted by altering the concentration of NaH_2PO_4.[28] Using this asymmetric template, Hao et al. fabricated spindle α-Fe_2O_3@SiO_2@polypyrrole sandwich composite nanoparticles with a spindle α-Fe_2O_3 core. By selectively removing the silica middle shell, a spindle hollow capsule with a movable hematite core was obtained.[29] Furthermore, by the carbonization-reduction process in vacuum, this spindle hollow capsule with a hematite core changed into hollow carbon nanocapsule with a movable magnetic core.[30] Sacanna et al. prepared fluorescent monodisperse spindle α-Fe_2O_3@SiO_2 core–shell nanoparticles for optical rotational diffusion studies.[31] Sánchez-Ferrer et al. fabricated inorganic–organic elastomer nanocomposites with spindle α-Fe_2O_3@SiO_2 as cross-linking agent.[32] Li et al. used spindle α-Fe_2O_3 as a core to prepare multifunctional α-Fe_2O_3@TiO_2 nanoparticle with uniform pores in TiO_2 shell.[33] Chen et al. reported a mesoporous nanoellipsoid with a spindle α-Fe_2O_3 core, which showed good performance in biological imaging and drug delivery.[11] These prior reports focused primarily on the fabrication of core–shell nanoparticles with spindle α-Fe_2O_3 as core, but the biological properties of the particles, including interaction with mammalian cells, have not been studied. As an easy prepared nonspherical nanoparticle, spindle α-Fe_2O_3 is an ideal model to explore the biological characteristics of nonspherical particles.

Given the ease of synthesis, the spindle α-Fe_2O_3 is an ideal model to be used in studying the biological characteristics of nonspherical particles. Here, we synthesized spindle hematite/polymer core–shell hybrid nanoparticles (SPNPs) via surface-initiated atom transfer radical polymerization (SI-ATRP) of oligo(ethylene glycol) methacrylate (OEGMA). The incorporation of poly(oligo(ethylene glycol) methacrylate) (POEGMA) covering the surface of the SPNPs was intended to reduce particle aggregation and to improve biocompatibility, so that the behavior of individual nonspherical particles in biological medium could be addressed without concerns due to instability. As shown in Scheme 1, we prepared the spindle hematite nanoparticles by hydrolysis of $Fe(NO_3)_3$ according to the literature.[28] The hematite particles were stabilized by poly(vinylpyrrolidone) (PVP) and then were covered with a layer of SiO_2 using the Stöber method.[34] The ATRP initiators were then introduced onto the hematite nanoparticles by two steps: (1) the reaction of 3-aminopropyl triethoxysilane (APTES) on the SiO_2 surface and (2) the coupling of 2-bromoisobutyryl bromide with APTES. The hydrophilic shell was formed by ATRP of OEGMA with a small amount of Rhodamine B

DOI: 10.1021/am509152h
ACS Appl. Mater. Interfaces 2015, 7, 5454–5461

methacrylate derivative to enable direct visualization and tracking of the nanoparticles by fluorescence microscopy. Last, HeLa cells were used to investigate the cellular uptake of the SPNPs.

2. MATERIALS AND METHODS

2.1. Materials. Iron(III) nitrate nonahydrate [$Fe(NO_3)_3 \cdot 9H_2O$] (≥98.5%, Westlong Chemical Reagent Co.), PVP (average M_w = 58 000, Alfa), APTES (98%, Alfa), ethyl 2-bromoisobutyrate (EBIB, 98%, Aldrich), 2,2′-bipyridine (99%, Alfa), 2-bromoisobutyryl bromide (98%, Aldrich), sodium dihydrogen phosphate (NaH_2PO_4, > 99%, Beijing Chemical Reagent Co.), and tetraethyl orthosilicate (TEOS, > 99%, Beijing Chemical Reagent Co.) were used as received. OEGMA (M_n = 475, 99%, Sigma-Aldrich) was purified by passing through a column packed with basic alumina to remove inhibitor. Copper(I) bromide (CuBr, Aldrich, 98%) was purified by stirring with glacial acetic acid followed by filtration and washing the solid three times with diethyl ether and then drying under vacuum. Rhodamine B methacrylate derivative (HEMA-Rhodamine B) was synthesized according to the literature.[35] 4,6-Diamidino-2-phenylindole (DAPI, Beyotime) was dissolved in a sodium phosphate buffer solution with the concentration of 2.5 μg/mL. Triethylamine (Beijing Chemical Reagent Co.) was dried over KOH. Toluene (>99%, Beijing Chemical Reagent Co.) was dried over Na. Chloroform (>99%, Beijing Chemical Reagent Co.) was dried over CaH_2. Other reagents were used as received without further purification.

2.2. Methods of Characterization. Thermogravimetric analysis (TGA) was performed using an SDT (simultaneous differential scanning calorimetry (DSC)-TGA) Q600 instrument under nitrogen atmosphere with a heating range of 25−700 °C at a heating rate of 20 °C/min. Fourier transform infrared (FT-IR) spectroscopy was recorded by a deuterate triglycine sulfate detector on a Bruker EQUINOX 55 spectrometer and was processed by the Bruker OPUS program. The samples were milled with potassium bromide (KBr) to form a fine powder and then were compressed into a thin pellet. Transmission electron microscopy (TEM) images were obtained using a JEOL JEM-1011 instrument operated at an accelerating voltage of 100 kV. The dispersed sample was dropped onto a carbon-coated copper grid and was dried at room temperature overnight. Confocal laser scanning microscopy (CLSM) images were taken with an Olympus FV1000-IX81 confocal system. The dispersed sample was dropped between two slides and was sealed with nail polish before observation. Light-scattering measurements were performed in aqueous dispersion of SPNPs at 150 μg/mL using a Zetasizer Nano Series (Malvern Instruments, U.K.) at 25 °C and were repeated three times. X-ray photoelectron spectroscopy (XPS) data were obtained with an ESCALab220i-XL electron spectrometer from VG Scientific using 300 W Al Kα radiation. The base pressure was 3×10^{-9} mbar. The binding energies were referenced to the C1s line at 284.8 eV from adventitious carbon.

2.3. Synthesis of Spindle α-Fe_2O_3. Spindle α-Fe_2O_3 was synthesized by a method described earlier.[28] Briefly, 4.4 g (0.01 mol) of $Fe(NO_3)_3 \cdot 9H_2O$ was dissolved in 250 mL distilled water. Under vigorous stirring, 1 M NaOH was added dropwise into the solution until the pH reached 10.5−10.8. The brown precipitate of $Fe(OH)_3$ was washed with distilled water 8−10 times until the pH was 9.3. The $Fe(OH)_3$ was dispersed in 200 mL water, and 20 mL of 0.1 M HCl and 2.25 mL of 0.1 M NaH_2PO_4 were added. The brown solution was transferred to a flask and was filled with distilled water to 500 mL. This final system was aged in an oil bath at 100 ± 2 °C for 2−3 days until the brown solution changed into a brick-red color. The precipitate was obtained by centrifugation followed by washing with distilled water several times.

2.4. Synthesis of Spindle α-Fe_2O_3@SiO_2. The 7.2 g PVP and 0.6 g spindle α-Fe_2O_3 were dispersed in 130 mL distilled water. Strong ultrasonication was applied for 20 min, and then the mixture was stirred for 24 h. The nanoparticles were obtained by centrifuging and washing with distilled water three times and with ethanol two times. The precipitate was dried under vacuum at room temperature for 24 h.

Silica was coated onto the α-Fe_2O_3 particles using the Stöber method.[34] An amount of 0.6 g PVP-stabilized α-Fe_2O_3 was added to a solution of 250 mL ethanol, 50 mL distilled water, and 6 mL ammonium hydroxide in a 500 mL round-bottom flask. Strong ultrasonication was applied for 20 min. Then the flask was immersed in an ice water bath. Under mechanical stirring, 0.6 mL TEOS was added. Then, the dispersion was stirred for 24 h at room temperature. The nanoparticles were obtained by centrifuging and washing with ethanol three times. The precipitate was dried under vacuum at room temperature for 24 h.

2.5. Synthesis of Spindle α-Fe_2O_3@SiO_2@NH_2. In a dried 50 mL round-bottom flask, 0.6 g α-Fe_2O_3@SiO_2 was added to 25 mL dried toluene. Strong ultrasonication was applied for 20 min. Under vigorous stirring, 3 mL APTES was added. The dispersion was stirred for 24 h at 80 °C. The nanoparticles were obtained by centrifuging and washing with toluene three times and with ethanol three times. The precipitate was dried under vacuum at room temperature for 24 h.

2.6. Synthesis of Spindle α-Fe_2O_3@SiO_2@Br. In a dried 50 mL round-bottom flask immersed in an ice water bath, 0.6 g α-Fe_2O_3@SiO_2@NH_2 was added to a solution of 30 mL dried chloroform and 4 mL triethylamine. Strong ultrasonication was applied for 20 min. Under vigorous stirring, 3 mL 2-bromoisobutyryl bromide and 10 mL dried chloroform were dripped slowly into the solution. The dispersion was stirred for 24 h. The nanoparticles were obtained by centrifuging and washing with chloroform three times and with ethanol three times. The precipitate was dried under vacuum at room temperature for 24 h.

2.7. Synthesis of POEGMA-Coated Rhodamine B Labeled SPNPs by ATRP. The polymerization procedure was as follows: α-Fe_2O_3@SiO_2@Br nanoparticles (0.06 g), EBIB (0.0078 g, 0.04 mmol), 2,2′-bipyridine (0.0249 g, 0.16 mmol), OEGMA (7.6 g, 16 mmol), HEMA-Rhodamine B (0.029 g, 0.049 mmol), and methanol (7.6 g) were added to a previously dried Schlenk tube equipped with a magnetic stir bar. Strong ultrasonication was applied for 20 min to give a well-dispersed solution. The tube was degassed by three freeze−evacuate−thaw cycles and was backfilled with N_2. As soon as CuBr (0.0115 g, 0.008 mmol) was introduced, the tube was vacuumed and flame-sealed. The tube was immersed into an oil bath at 60 °C for 24 h with vigorous stirring, and then the reaction mixture was exposed to the air and was further diluted with methanol. The nanoparticles were obtained by centrifuging and washing with methanol three times and with distilled water three times. Then, the precipitate was dispersed in water with ultrasonication and was dialyzed against water for 3 days.

DOI: 10.1021/am509152h
ACS Appl. Mater. Interfaces 2015, 7, 5454−5461

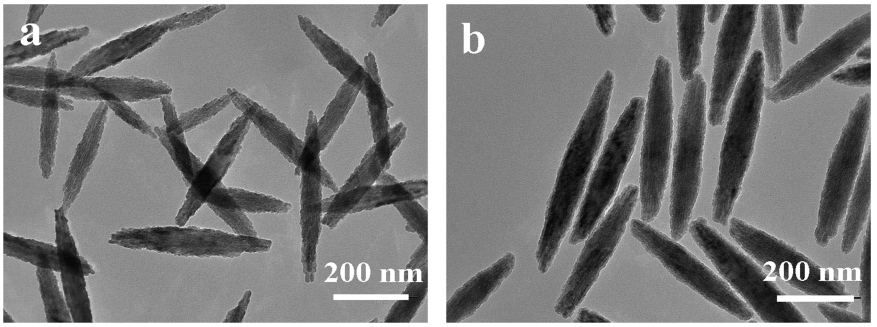

Figure 1. TEM images of (a) spindle α-Fe_2O_3 and (b) spindle α-Fe_2O_3@SiO_2.

2.8. Intracellular Uptake of SPNPs. HeLa cells were seeded onto a 35 mm glass-bottom Petri dish at a density of 10 000 cells/cm^2 and were incubated in a humidified atmosphere of 5% CO_2 at 37 °C. After 24 h, the cells were treated with 2 mL Rhodamine B labeled SPNPs at a final concentration of 150 μg/mL. At different time points of culture at 37 °C, the cells were washed three times with cold PBS (pH 7.4) to remove free SPNPs and then were fixed with 1 mL of 4% paraformaldehyde for 20−30 min at 37 °C. After washing three times with PBS, the nuclei of the cells were stained with 1 mL of DAPI and were incubated at 37 °C. Then, the cells were washed three times with PBS, were sealed, and were kept at 4 °C until confocal imaging. CLSM images were obtained by an Olympus FV1000-IX81 confocal system, equipped with an argon laser. DAPI was visualized with excitation and emission wavelengths of 405 and 450 nm, respectively. Rhodamine B was visualized with excitation and emission wavelengths of 559 and 595 nm, respectively.

3. RESULTS AND DISCUSSION

3.1. Preparation and Characterization of SPNPs. Spindle α-Fe_2O_3 nanoparticles with narrow size dispersity were synthesized by hydrolysis of $Fe(NO_3)_3{\cdot}9H_2O$ at 100 °C for 2−3 days according to a method reported previously.[28] Figure 1a shows the TEM image of spindle α-Fe_2O_3 with measured dimensions of 352 ± 64 nm for the longer axis and 61 ± 13 nm for the shorter axis. Then, the α-Fe_2O_3 particle, as a core, was stabilized by PVP for better silica coating. The PVP coating prevented the α-Fe_2O_3 particles from aggregation.[34] Silica-coated α-Fe_2O_3 particles were formed in a seeded growth process following the Stöber method. The morphology of the α-Fe_2O_3@SiO_2 was still spindle-shaped, as shown in Figure 1b. The thickness of the silica layer was about 10 nm.

α-Fe_2O_3@SiO_2@NH_2 was prepared by the reaction of α-Fe_2O_3@SiO_2 and silane coupling agent APTES. XPS was used to confirm the amino groups grafted onto the particle surface. Figure 2a shows the XPS wide scan spectrum of α-Fe_2O_3@SiO_2@NH_2. The percentage of nitrogen element was calculated to be 5.76%. Then, the α-Fe_2O_3@SiO_2@NH_2 reacted with 2-bromoisobutyryl bromide to obtain α-Fe_2O_3@SiO_2@Br. Figure 2b shows the XPS spectrum of α-Fe_2O_3@SiO_2@Br. The appearance of strong Br 3d and Br 3p signals confirmed the presence of Br on the particle surface, which acted as the initiator for the subsequent SI-ATRP to create a polymer shell. The percentage of Br element was calculated to be 1.27%.

Polyethylene glycol (PEG) has been widely used in biological, chemical, and pharmaceutical fields because of its good aqueous solubility and biocompatibility. When grafted onto a particle surface, PEG can help reduce the toxicity of the particle and avoid clearance by the reticuloendothelium, thus prolonging the circulation time of the particle.[36] In this work, PEG-containing segment OEGMA was grafted onto the spindle α-Fe_2O_3 particles via SI-ATRP. The grafted POEGMA was expected to not only increase the biocompability of α-Fe_2O_3 particles but also improve their dispersion in aqueous media.

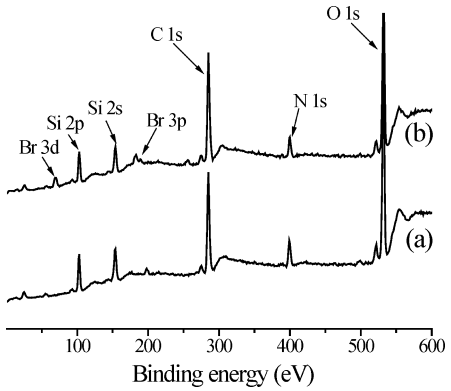

Figure 2. XPS wide scan spectra of (a) α-Fe_2O_3@SiO_2@NH_2 and (b) α-Fe_2O_3@SiO_2@Br.

The morphology of polymer-grafted nanoparticles (SPNPs) remained as spindle-shaped after the polymerization (Figure 3a). The long axis of the SPNPs was 370 ± 65 nm, and the short axis was 80 ± 15 nm with an aspect ratio of 4.6−4.7. The thickness of the grafted polymer was about 10 nm according to the TEM images. The SPNPs were fluorescently labeled by adding a small amount of HEMA-Rhodamine B during the polymerization. Figure 3b shows the CLSM image of the SPNPs dispersed very well in water without any aggregation. FT-IR was used to confirm the grafting of POEGMA. The strong band at 570 cm^{-1} was related to the Fe−O stretches in α-Fe_2O_3 (Figure 4, line a).[37] After modified by PVP (Figure 4, line b), the typical bond absorptions appeared at 1284 and

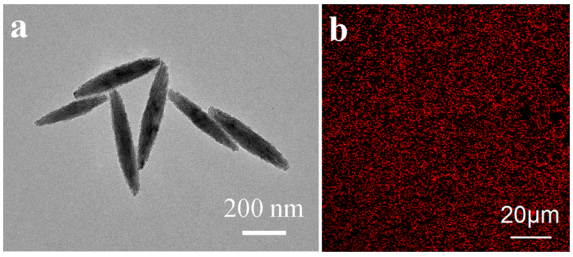

Figure 3. (a) TEM image of the SPNPs and (b) CLSM image of the Rhodamine B labeled SPNPs.

DOI: 10.1021/am509152h
ACS Appl. Mater. Interfaces 2015, 7, 5454−5461

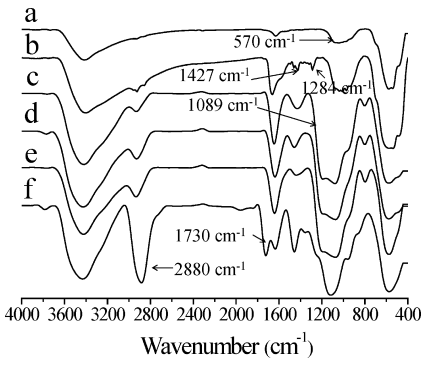

Figure 4. FT-IR spectra of (a) α-Fe_2O_3, (b) α-Fe_2O_3@PVP, (c) α-Fe_2O_3@SiO_2, (d) α-Fe_2O_3@SiO_2@NH_2, (e) α-Fe_2O_3@SiO_2@Br, and (f) SPNPs.

1427 cm^{-1}, which were the absorptions of N → H−O and the pyridine ring.[38] For SiO_2 coated particles, the band at 1089 cm^{-1} was associated with Si−O−Si stretching vibration (Figure 4, line c).[39] The peak at 1730 cm^{-1} was characteristic of the C═O bond of POEGMA, and the peak at 2880 cm^{-1} was attributed to the saturated C−H bond of POEGMA (Figure 4, line f).[40] The evidence indicated that the POEGMA chains were grafted onto the particles successfully.

The mass fraction of the grafted POEGMA was determined by TGA. The SPNPs showed an apparent weight loss in the range of 200−400 °C (Figure 5). The weight loss of α-Fe_2O_3@

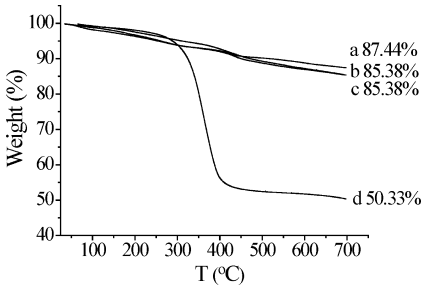

Figure 5. TGA curves of (a) α-Fe_2O_3@SiO_2, (b) α-Fe_2O_3@SiO_2@NH_2, (c) α-Fe_2O_3@SiO_2@Br, and (d) SPNPs.

SiO_2@Br was 14.6% and that of SPNPs was 49.7% at 700 °C. The difference in the weight retention between them indicates the existence of the grafted polymers. The weight fraction of grafted polymer was calculated as 41.1%, according to $(M_2 - M_1)/M_2$, where M_1 is the weight of α-Fe_2O_3@SiO_2@Br and M_2 is the weight of SPNPs.

Dynamic light scattering measurement was used to evaluate the average size distribution of the SPNPs in aqueous solutions. The dispersity of SPNPs in water was narrow (PDI 0.056), and the average diameter was 209 nm (Figure 6a). The SPNPs have a slightly negative surface charge in water with a zeta potential of −9.74 mV. The dispersibility of SPNPs in cell culture medium (DMEM containing 10% FBS and 1% penicillin-streptomycin) was also evaluated by DLS. As shown in Figure 6b, the average diameter of SPNPs was 219 nm and the PDI was 0.064, indicating that the SPNPs dispersed equally well in serum-containing DMEM as in pure water with a very slight (<5%) increase in size.

3.2. Cellular Uptake of SPNPs. The interaction between HeLa cells and SPNPs was investigated. We incubated the SPNPs with HeLa cells at a particle concentration of 300 μg/mL for various times (1, 4, 8, 12, and 24 h), and the cells were then observed by CLSM. As shown in Figure 7, the images from top to bottom refer to DAPI-labeled nuclei, Rhodamine-B-labeled SPNPs, and their superimposition, respectively. It was found that at earlier time points (1 and 4 h), the SPNPs were primarily found at the vicinity of the cell membrane, indicating the beginning of the cellular uptake process. As time increased to 8 h, the amount of SPNPs found in the cytoplasm of HeLa cells gradually increased, suggesting that the internalized particles were being transported to the deeper interior of cells. Beyond 8 h, however, the amount of internalized SPNPs did not show any significant increase, indicating that the cellular uptake process had reached equilibrium. Despite substantial intracellular uptake, few SPNPs were found inside the cell nuclei even as late as 24 h (Figure 7). Furthermore, the time-course cell uptake was evaluated by quantitative analysis (Figure 8). The average fluorescence area of 100 cells based on CLSM images was estimated in Image-Pro Plus 6.0 software to obtain the quantitative data. We found that the average fluorescence area gradually increased and grew to a maximum in 8 h. Then, the average fluorescence area decreased slightly in the next 16 h, which could be due to the exocytosis and the fluorescence quenching. Hao et al. reported that the uptake amount of mesoporous silica nanoparticles (diameter × length: 115 ± 15 nm × 218 ± 21 nm and 136 ± 28 nm × 558 ± 43 nm) with different aspect ratios by HeLa cells increased and reached a maximum in 2 h.[41] Another report suggested that the uptake amount of disklike particles (diameter × height: 325 nm × 100 nm) by HeLa cells increased continuously for 72 h.[17] However, we got a different result of SPNPs uptake by HeLa cells, which could be caused by the different shapes and surface properties of the particles.

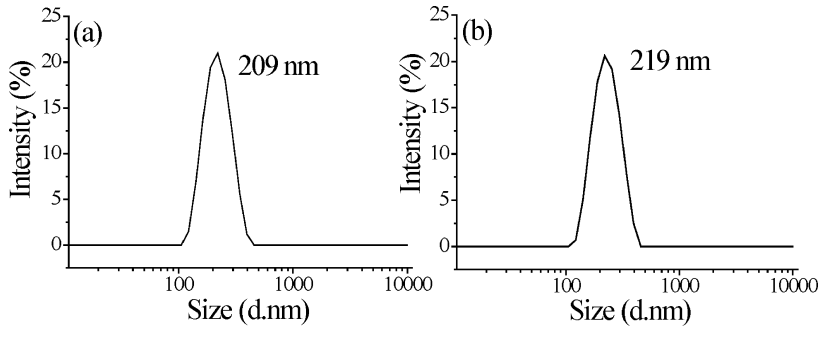

Figure 6. Size distribution by intensity of SPNPs in (a) water and (b) cell culture medium DMEM.

DOI: 10.1021/am509152h
ACS Appl. Mater. Interfaces 2015, 7, 5454−5461

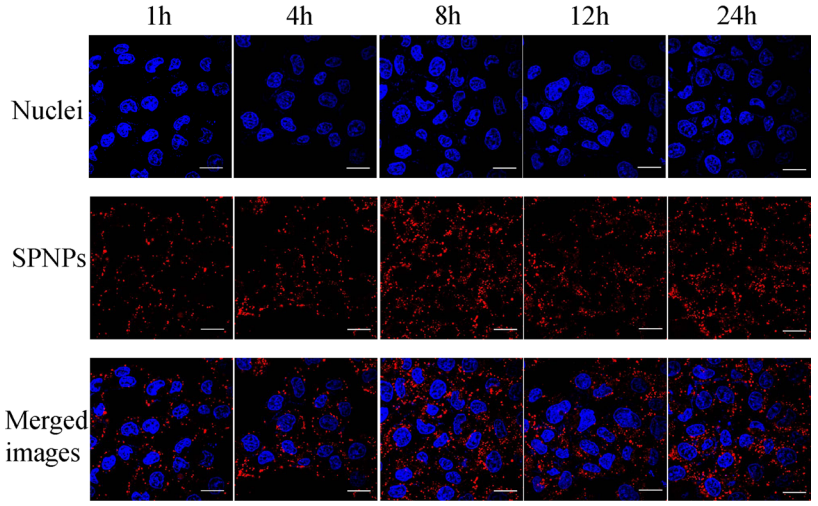

Figure 7. CLSM images of SPNPs coculturing with HeLa cells at different times. Bar: 20 μm.

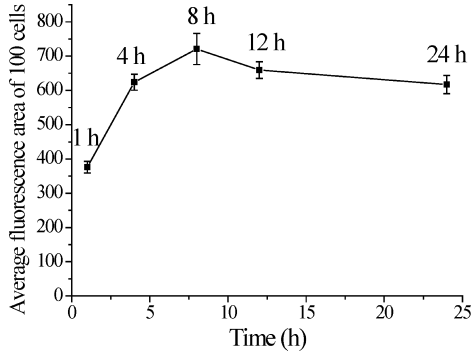

Figure 8. Quantitative analysis of time-course SPNPs uptake by HeLa cells.

Finally, TEM was used to provide unequivocal evidence for the intracellular uptake of SPNPs. The SPNPs were coculturing with HeLa cells for 24 h and were collected for TEM observation. Figure 9 shows the location of the SPNPs in the cells. It was found that the SPNPs were mainly located in the cytoplasm as discrete, individual particles. It was noticed that the SPNPs were located in the vesicles of the cytoplasm as shown in the magnified images of Figure 10. It was also found

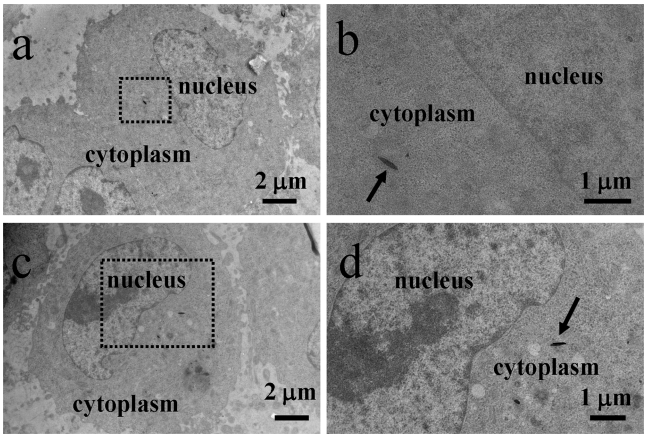

Figure 9. TEM images of HeLa cells coculturing with the SPNPs after (a, c) 24 h . (b, d) The enlarged rectangular areas of a and c.

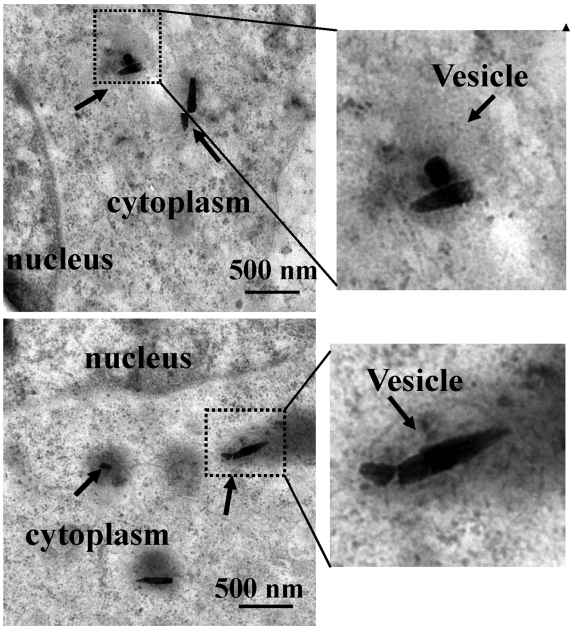

Figure 10. TEM images of HeLa cells coculturing with the SPNPs after 24 h.

that the SPNPs in the vesicles do not seem to be perfectly spindle shaped and have rougher edges; also, some were broken, as shown by the black arrows in Figure 10. This may indicate that intracellular degradation of the particles was in progress, as endolysosomal enzymes and acidic pH are both expected to digest the polymer shell and the iron oxide core, leading to fracture of the SPNPs. This finding suggests that the polymer nanoparticles could be digested by cells.

4. CONCLUSIONS

In summary, SPNPs were prepared by SI-ATRP using spindle α-Fe_2O_3 as a template core. The POEGMA-containing polymer chains grafted onto the surface of α-Fe_2O_3 with a content of 41.1% by weight. TEM confirmed the nonspherical spindle shape of the SPNPs with the long axis of 370 ± 65 nm and the short axis of 80 ± 15 nm and the aspect ratio of 4.6−4.7. The SPNPs were quickly internalized by HeLa cells within 1 h, and the uptake reached equilibrium in 8 h. The internalized SPNPs

DOI: 10.1021/am509152h
ACS Appl. Mater. Interfaces 2015, 7, 5454−5461

were located as discrete particles in the vesicles of the cytoplasm, and few particles were found in the cell nuclei. Fractured SPNPs inside cells were visualized by TEM for the first time, which may indicate the intermediate stage of breaking-down of the nanoparticles because of digestion by endolysosomal enzymes and acidic pH. These nonspherical spindle-shaped hematite/polymer hybrid nanoparticles with well-defined polymer shell synthesized by living polymerization may be useful model systems for mechanistic studies of nanoparticle/cell interaction. Furthermore, observations of intracellular uptake of these particles in this report may be valuable to improving the design of nanocarriers for intracellular drug delivery.

AUTHOR INFORMATION

Corresponding Authors

*E-mail: berry_zw@iccas.ac.cn.
*E-mail: liulixin@mail.sysu.edu.cn.
*E-mail: ymchen@iccas.ac.cn.

Notes

The authors declare no competing financial interest.

ACKNOWLEDGMENTS

We would like to thank Yanxia Jia and Lei Sun of the Center for Biological Imaging (CBI), Institute of Biophysics, Chinese Academy of Science for their kindly help in taking TEM images of cells. Financial support by the National Science Foundation of China (21090353 and 51203171) and Guangdong Innovative and Entepreneurial Research Team Program (2013S086) is gratefully acknowledged.

REFERENCES

(1) Soppimath, K. S.; Aminabhavi, T. M.; Kulkarni, A. R.; Rudzinski, W. E. Biodegradable Polymeric Nanoparticles as Drug Delivery Devices. *J. Controlled Release* **2001**, *70*, 1−20.

(2) Xiao, K.; Luo, J.; Li, Y.; Xiao, W.; Lee, J. S.; Gonik, A. M.; Lam, K. S. The Passive Targeting of Polymeric Micelles in Various Types and Sizes of Tumor Models. *Nanosci. Nanotechnol. Lett.* **2010**, *2*, 79−85.

(3) Elsabahy, M.; Wooley, K. L. Design of Polymeric Nanoparticles for Biomedical Delivery Applications. *Chem. Soc. Rev.* **2012**, *41*, 2545−2561.

(4) Cheng, R.; Meng, F.; Deng, C.; Klok, H.-A.; Zhong, Z. Dual and Multi-stimuli Responsive Polymeric Nanoparticles for Programmed Site-specific Drug Delivery. *Biomaterials* **2013**, *34*, 3647−3657.

(5) Crucho, C. I. C. Stimuli-Responsive Polymeric Nanoparticles for Nanomedicine. *ChemMedChem.* **2015**, *10*, 24−38.

(6) Savić, R.; Luo, L. B.; Eisenberg, A.; Maysinger, D. Micellar Nanocontainers Distribute to Defined Cytoplasmic Organelles. *Science* **2003**, *300*, 615−618.

(7) Geng, Y.; Dalhaimer, P.; Cai, S.; Tsai, R.; Tewari, M.; Minko, T.; Discher, D. E. Shape Effects of Filaments versus Spherical Particles in Flow and Drug Delivery. *Nat. Nanotechnol.* **2007**, *2*, 249−255.

(8) Gratton, S. E. A.; Ropp, P. A.; Pohlhaus, P. D.; Luft, J. C.; Madden, V. J.; Napier, M. E.; DeSimone, J. M. The Effect of Particle Design on Cellular Internalization Pathways. *Proc. Natl. Acad. Sci. U.S.A.* **2008**, *105*, 11613−11618.

(9) Meng, H.; Yang, S.; Li, Z.; Xia, T.; Chen, J.; Ji, Z.; Zhang, H.; Wang, X.; Lin, S.; Huang, C.; Zhou, Z. H.; Zink, J. I.; Nel, A. E. Aspect Ratio Determines the Quantity of Mesoporous Silica Nanoparticle Uptake by a Small GTPase-Dependent Macropinocytosis Mechanism. *ACS Nano* **2011**, *5*, 4434−4447.

(10) Hao, N.; Yang, H.; Li, L.; Li, L.; Tang, F. The Shape Effect of Mesoporous Silica Nanoparticles on Intracellular Reactive Oxygen Species in A375 Cells. *New J. Chem.* **2014**, *38*, 4258−4266.

(11) Chen, Y.; Chen, H.; Zhang, S.; Chen, F.; Zhang, L.; Zhang, J.; Zhu, M.; Wu, H.; Guo, L.; Feng, J.; Shi, J. Multifunctional Mesoporous Nanoellipsoids for Biological Bimodal Imaging and Magnetically Targeted Delivery of Anticancer Drugs. *Adv. Funct. Mater.* **2011**, *21*, 270−278.

(12) Zhang, Y.; Tekobo, S.; Tu, Y.; Zhou, Q.; Jin, X.; Dergunov, S. A.; Pinkhassik, E.; Yan, B. Permission to Enter Cell by Shape: Nanodisk vs Nanosphere. *ACS Appl. Mater. Interfaces* **2012**, *4*, 4099−4105.

(13) Fan, J.-B.; Song, Y.; Li, H.; Jia, J.-P.; Guo, X.; Jiang, L. Controllable Drug Release and Effective Intracellular Accumulation Highlighted by Anisotropic Biodegradable PLGE Nanoparticles. *J. Mater. Chem. B* **2014**, *2*, 3911−3914.

(14) Alemdaroglu, F. E.; Alemdaroglu, N. C.; Langguth, P.; Herrmann, A. Cellular Uptake of DNA Block Copolymer Micelles with Different Shapes. *Macromol. Rapid Commun.* **2008**, *29*, 326−329.

(15) Huang, X.; Teng, X.; Chen, D.; Tang, F.; He, J. The Effect of the Shape of Mesoporous Silica Nanoparticles on Cellular Uptake and Cell Function. *Biomaterials* **2010**, *31*, 438−448.

(16) Chithrani, B. D.; Chan, W. C. W. Elucidating the Mechanism of Cellular Uptake and Removal of Protein-coated Gold Nanoparticles of Different Sizes and Shapes. *Nano Lett.* **2007**, *7*, 1542−1550.

(17) Agarwal, R.; Singh, V.; Jurney, P.; Shi, L.; Sreenivasan, S. V.; Roy, K. Mammalian Cells Preferentially Internalize Hydrogel Nanodiscs over Nanorods and Use Shape-specific Uptake Mechanisms. *Proc. Natl. Acad. Sci. U.S.A.* **2013**, *110*, 17247−17252.

(18) Decuzzi, P.; Godin, B.; Tanaka, T.; Lee, S. Y.; Chiappini, C.; Liu, X.; Ferrari, M. Size and Shape Effects in the Biodistribution of Intravascularly Injected Particles. *J. Controlled Release* **2010**, *141*, 320−327.

(19) Devarajan, P. V.; Jindal, A. B.; Patil, R. R.; Mulla, F.; Gaikwad, R. V.; Samad, A. Particle Shape: A New Design Parameter for Passive Targeting in Splenotropic Drug Delivery. *J. Pharm. Sci.* **2010**, *99*, 2576−2581.

(20) Arnida; Janat-Amsbury, M. M.; Ray, A.; Peterson, C. M.; Ghandehari, H. Geometry and Surface Characteristics of Gold Nanoparticles Influence Their Biodistribution and Uptake by Macrophages. *Eur. J. Pharm. Biopharm.* **2011**, *77*, 417−423.

(21) Christian, D. A.; Cai, S.; Garbuzenko, O. B.; Harada, T.; Zajac, A. L.; Minko, T.; Discher, D. E. Flexible Filaments for in Vivo Imaging and Delivery: Persistent Circulation of Filomicelles Opens the Dosage Window for Sustained Tumor Shrinkage. *Mol. Pharmaceutics* **2009**, *6*, 1343−1352.

(22) Gentile, F.; Chiappini, C.; Fine, D.; Bhavane, R. C.; Peluccio, M. S.; Cheng, M. M.-C.; Liu, X.; Ferrari, M.; Decuzzi, P. The Effect of Shape on the Margination Dynamics of Non-neutrally Buoyant Particles in Two-dimensional Shear Flows. *J. Biomech.* **2008**, *41*, 2312−2318.

(23) Lee, S.-Y.; Ferrari, M.; Decuzzi, P. Design of Bio-mimetic Particles with Enhanced Vascular. *Interact. J. Biomech.* **2009**, *42*, 1885−1890.

(24) Shah, S.; Liu, Y.; Hu, W.; Gao, J. Modeling Particle Shape-Dependent Dynamics in Nanomedicine. *J. Nanosci. Nanotechnol.* **2011**, *11*, 919−928.

(25) Nangia, S.; Sureshkumar, R. Effects of Nanoparticle Charge and Shape Anisotropy on Translocation through Cell Membranes. *Langmuir* **2012**, *28*, 17666−17671.

(26) Huang, C.; Zhang, Y.; Yuan, H.; Gao, H.; Zhang, S. Role of Nanoparticle Geometry in Endocytosis: Laying Down to Stand Up. *Nano Lett.* **2013**, *13*, 4546−4550.

(27) Matijević, E.; Scheiner, P. Ferric Hydrous Oxide Sols III. Preparation of Uniform Particles by Hydrolysis of Fe(III)-Chloride, Fe(III)-Nitrate, and Fe(III)-Perchlorate Solution. *J. Colloid Interface Sci.* **1978**, *63*, 509−524.

(28) Ocaña, M.; Morales, M. P.; Serna, C. J. Homogeneous Precipitation of Uniform Alpha-Fe_2O_3 Particles from Iron Salts Solutions in the Presence of Urea. *J. Colloid Interface Sci.* **1999**, *212*, 317−323.

DOI: 10.1021/am509152h
ACS Appl. Mater. Interfaces 2015, 7, 5454−5461

(29) Hao, L. Y.; Zhu, C. L.; Jiang, W. Q.; Chen, C. N.; Hu, Y.; Chen, Z. Y. Sandwich Fe_2O_3@SiO_2@PPy Ellipsoidal Spheres and Four Types of Hollow Capsules by Hematite Olivary Particles. *J. Mater. Chem.* **2004**, *14*, 2929−2934.
(30) Hao, L.-Y.; Xuan, S.-H.; Gong, X.-L.; Gu, R.; Jiang, W.-Q.; Chen, Z.-Y. Ellipsoidal Carbon Capsules Encapsulated Magnetite Nanorods. *Chem. Lett.* **2007**, *36*, 126−127.
(31) Sacanna, S.; Rossi, L.; Kuipers, B. W. M.; Philipse, A. P. Fluorescent Monodisperse Silica Ellipsoids for Optical Rotational Diffusion Studies. *Langmuir* **2006**, *22*, 1822−1827.
(32) Sánchez-Ferrer, A.; Reufer, M.; Mezzenga, R.; Schurtenberger, P.; Dietsch, H. Inorganic-organic Elastomer Nanocomposites from Integrated Ellipsoidal Silica-coated Hematite Nanoparticles as Cross-linking Agents. *Nanotechnology* **2010**, *21*, 185603.
(33) Li, W.; Yang, J.; Wu, Z.; Wang, J.; Li, B.; Feng, S.; Deng, Y.; Zhang, F.; Zhao, D. A Versatile Kinetics-Controlled Coating Method To Construct Uniform Porous TiO_2 Shells for Multifunctional Core-Shell Structures. *J. Am. Chem. Soc.* **2012**, *134*, 11864−11867.
(34) Graf, C.; Vossen, D. L. J.; Imhof, A.; van Blaaderen, A. A General Method to Coat Colloidal Particles with Silica. *Langmuir* **2003**, *19*, 6693−6700.
(35) Wakizono, S.; Yamamoto, K.; Kadokawa, J.-i. FRET Function of Polymeric Ionic Liquid Film Containing Rhodamine Moieties for Exhibiting Emissions by Excitation at Wide Wavelength Areas. *J. Photochem. Photobiol., A* **2011**, *222*, 283−287.
(36) Leroux, J. C.; Allémann, E.; DeJaeghere, F.; Doelker, E.; Gurny, R. Biodegradable Nanoparticles - From Sustained Release Formulations to Improved Site Specific Drug Delivery. *J. Controlled Release* **1996**, *39*, 339−350.
(37) Xuan, S.; Fang, Q.; Hao, L.; Jiang, W.; Gong, X.; Hu, Y.; Chen, Z. Fabrication of Spindle Fe_2O_3@polypyrrole Core/shell Particles by Surface-modified Hematite Templating and Conversion to Spindle Polypyrrole Capsules and Carbon Capsules. *J. Colloid Interface Sci.* **2007**, *314*, 502−509.
(38) Zhang, J.; Liu, H.; Wang, Z.; Ming, N. Au-induced Polyvinylpyrrolidone Aggregates with Bound Water for the Highly Shape-selective Synthesis of Silica Nanostructures. *Chem.—Eur. J.* **2008**, *14*, 4374−4380.
(39) Li, Q.; Zhang, L.; Zhang, Z.; Zhou, N.; Cheng, Z.; Zhu, X. Air-Tolerantly Surface-Initiated AGET ATRP Mediated by Iron Catalyst from Silica Nanoparticles. *J. Polym. Sci., Part A: Polym. Chem.* **2010**, *48*, 2006−2015.
(40) Li, G.; Zeng, D. L.; Wang, L.; Zong, B.; Neoh, K. G.; Kang, E. T. Hairy Hybrid Nanoparticles of Magnetic Core, Fluorescent Silica Shell, and Functional Polymer Brushes. *Macromolecules* **2009**, *42*, 8561−8565.
(41) Hao, N.; Li, L.; Zhang, Q.; Huang, X.; Meng, X.; Zhang, Y.; Chen, D.; Tang, F.; Li, L. The Shape Effect of PEGylated Mesoporous Silica Nanoparticles on Cellular Uptake Pathway in Hela Cells. *Microporous Mesoporous Mater.* **2012**, *162*, 14−23.

DOI: 10.1021/am509152h
ACS Appl. Mater. Interfaces 2015, 7, 5454−5461